General Disclaimer

One or more of the Following Statements may affect this Document

- This document has been reproduced from the best copy furnished by the organizational source. It is being released in the interest of making available as much information as possible.

- This document may contain data, which exceeds the sheet parameters. It was furnished in this condition by the organizational source and is the best copy available.

- This document may contain tone-on-tone or color graphs, charts and/or pictures, which have been reproduced in black and white.

- This document is paginated as submitted by the original source.

- Portions of this document are not fully legible due to the historical nature of some of the material. However, it is the best reproduction available from the original submission.

NASA Technical Memorandum 83333
AIAA-83-0759

Application of 3-Signal Coherence to Core Noise Transmission

Eugene A. Krejsa
Lewis Research Center
Cleveland, Ohio

Prepared for the
Eighth Aeroacoustics Conference
sponsored by the American Institute of Aeronautics and Astronautics
Atlanta, Georgia, April 11-13, 1983

NASA

APPLICATION OF 3-SIGNAL COHERENCE TO CORE NOISE TRANSMISSION

Eugene A. Krejsa
National Aeronautics and Space Administration
Lewis Research Center
Cleveland, Ohio 44135

Abstract

A method for determining transfer functions across turbofan engine components and from the engine to the far-field is developed. The method is based on the 3-signal coherence technique used previously to obtain far-field core noise levels. This method eliminates the bias error in transfer function measurements due to contamination of measured pressures by nonpropagating pressure fluctuations. Measured transfer functions from the engine to the far-field, across the tailpipe, and across the turbine are presented for three turbofan engines.

Introduction

One of the sources of noise from turbine powered aircraft that can be a significant contributor to the total noise of the aircraft is core noise (Ref. 1). Core noise is usually considered to originate in the engine combustor. One mechanism often assumed to produce core noise is unsteady heat release. Strahle (Ref. 2) also considered turbulence vorticity as a source of core noise. The noise generated in the combustor must propagate across the turbine, through the tailpipe, and then radiate to the far-field. The propagation mechanism need not be solely acoustic. For the case of core noise generation by unsteady heat release, both pressure and entropy fluctuations are generated. The pressure fluctuations propagate acoustically while the entropy fluctuations convect with the flow. As these entropy fluctuations convect through regions of velocity or density gradients additional pressure waves are generated. Thus the pressure downstream of a region with velocity or density gradients results from a combination of acoustic and convective propagation. An important quantity can be defined which relates the pressure downstream of a region to the pressure upstream of the region. This quantity is the pressure-to-pressure transfer function across the region.

In this report engine component transfer functions computed from measured pressure fluctuations are presented for several turbofan engines. The transfer functions presented are: from the engine tailpipe exit to the far-field, across the engine tailpipe, and across the turbine. These transfer functions are determined using a technique based on the 3-signal coherence technique used previously (Ref. 3), to obtain far-field core noise levels. The technique eliminates the bias error in transfer function measurements due to the contamination of measured pressures by nonpropagating pressure fluctuations, i.e., pseudosound.

Nomenclature

A_E	area of engine core exit, m^2
C_E	speed of sound at engine core exit, m/s
C_o	ambient speed of sound, m/s
f	frequency, Hz
G_{mm}, G_{uu}, G_{xx}	auto-spectra of variables m(t), u(t), and x(t), respectively
G_{mn}, G_{mp}, G_{np}	cross-spectra between variables denoted by subscripts
G_{uv}, G_{uw}, G_{vw}	cross-spectra between variables denoted by subscripts
G_{xy}, G_{xz}, G_{yz}	cross-spectra between variables denoted by subscripts
H	true transfer function
H_m	estimated transfer function
H_{uv}, H_{vw}	transfer function between u and v, and v and w, respectively
M, N, P	Fourier transforms of m, n, and p, respectively
m, n, p	extraneous noise at inputs and outputs in time domain
M_E	Mach number at core exit
$\lvert P_E \rvert$	magnitude of pressure at core exit, N/m^2
$\lvert \overline{P}_F \rvert$	magnitude of area weighted average far-field pressure, N/m^2
R	far-field measurement distance, m
t	time, sec
U, V, W	Fourier transforms of u, v, and w, respectively
u, v, w	noise-free time domain signals at inputs and outputs
x, y, z	measured time domain signals at inputs and outputs, defined by Eqs. (1), (2), and (3), respectively
Z_E	ratio of core exit impedance to $\rho_E C_E$
ρ_E	density at core exit, kg/m^3
ρ_o	ambient density, kg/m^3

Superscripts:

*	complex conjugate
overbar	expected value

Transfer Function Measurement Technique

Background

The true transfer function of a system is defined as the amplitude ratio and phase difference between the output of a system and the input that produced the output.

For a system whose input is a random variable, the transfer function of the system can be estimated using random data analysis techniques. If extraneous noise exists at the input to the system, i.e., noise at the input that does not produce an output, the transfer function determined using the usual random data analysis equations will be biased. In Ref. 4, the equations for a single input/single output system with extraneous noise are given. The analysis of that system will be presented here to show how the extraneous input noise biases the estimate of the true transfer function. A schematic of the single input/single output system, from Ref. 4, is shown in Fig. 1. Here, $u(t)$ is the signal at the input to the system, $m(t)$ is the extraneous noise at the input, and $x(t)$ is the total measured signal at the input, so that

$$x(t) = u(t) + m(t) \tag{1}$$

The corresponding signals at the output are $v(t)$, $n(t)$, and $y(t)$, thus

$$y(t) = v(t) + n(t) \tag{2}$$

$H(f)$ is the desired system transfer function relating the Fourier transform of the output to the Fourier transform of the input, and is expressed by

$$H(f) = \frac{V(f)}{U(f)} = \frac{G_{uv}(f)}{G_{uu}(f)} \tag{3}$$

where $V(f)$ and $U(f)$ are the Fourier transforms of $v(t)$ and $u(t)$, respectively, G_{uv} is the cross-spectrum between $u(t)$ and $v(t)$, and G_{uu} is the auto-spectrum of $u(t)$. However, $v(t)$ and $u(t)$ cannot be measured by themselves. The measurable quantities are $x(t)$ and $y(t)$. However, these quantities contain the contaminating signals $m(t)$ and $n(t)$. An estimate of the true transfer function can be made using the measured quantities x and y and Eq. (4).

$$H_m(f) = \frac{G_{xy}(f)}{G_{xx}(f)} \tag{4}$$

where G_{xy} is the cross-spectrum between x and y and G_{xx} us the auto-spectrum of x. The measured transfer function, H_m, is related to the true transfer function, H, by the following equation:

$$H_m(f) = \frac{G_{xy}(f)}{G_{xx}(f)} = \frac{G_{uv} + G_{mn}}{G_{uu} + G_{mm}} = H \frac{\left(1 + \dfrac{G_{mn}}{G_{uv}}\right)}{1 + \dfrac{G_{mm}}{G_{uu}}} \tag{5}$$

Thus, due to the extraneous noise at the input and the correlation between this noise and the extraneous noise at the output, the measured transfer function is a biased estimate of the true transfer function. Even for the case of uncorrelated input and output noise, the existence of extraneous noise at the input produces a biased estimate of the transfer function.

For the situation where the transfer function within the core of a turbofan engine or from the core to the far-field is desired, the measured pressure fluctuations are almost certain to contain extraneous noise. The extraneous noise at two locations within the engine may or may not be correlated. However, based on the preceding discussion, any extraneous noise at the input to a system will produce a biased estimate of the transfer function whether or not the extraneous noise at the input correlates with that at the output. In the next section, a technique for determining the unbiased transfer function will be developed.

Unbiased Transfer Function Determination

Shown in Fig. 2, is a schematic of a system similar to that shown in Fig. 1 except that another block has been added. The output of that block is $w(t)$. Extraneous noise, $p(t)$, is assumed to exist at the output of this new block and the measured quantity at the output is $z(t)$, thus

$$z(t) = w(t) + p(t) \tag{6}$$

If $z(t)$ is an acoustic signal measured in the far-field of an engine, and $w(t)$ is defined as that portion that correlates with the signals measured in the core, then, by definition $p(t)$ will not correlate with either $m(t)$ or $n(t)$. Thus;

$$G_{mp} = \overline{M^*P} = 0 \qquad G_{np} = \overline{N^*P} = 0 \tag{7}$$

and

$$G_{xz} = G_{uw} = \overline{U^*W} \tag{8}$$

and

$$G_{yz} = G_{vw} = \overline{V^*W} \tag{9}$$

Here, the capitalized symbols represent the Fourier transform of the (lower case) time domain variable, the asterisk denotes the complex conjugate, and the overbar indicates the expected value obtained by ensemble averaging.

Dividing the conjugate of the cross-spectrum between y and z, G^*_{yz}, by the conjugate of the cross-spectrum between x and z, G^*_{xz}, gives:

$$\frac{G^*_{yz}}{G^*_{xz}} = \frac{\overline{VW^*}}{\overline{UW^*}} = \frac{\overline{V}}{\overline{U}} = H_{uv} \tag{10}$$

H_{uv} is the desired transfer function of the component represented by the first block in Fig. 2. Thus this transfer function between u and v can be determined, using Eq. (10), without any bias errors due to contaminating noise by using an additional measurement.

A similar analysis can now be made to obtain the transfer function across the second block, H_{vw}. The cross-spectrum between x and y is given by

$$G_{xy} = G_{uv} + G_{mn} \tag{11}$$

where the second term results from the possible correlation of the contaminating signals m and n. The cross-spectrum between x and z is given by

$$G_{xz} = G_{uw} \tag{12}$$

No term involving the contaminating signals is present because they do not correlate. Dividing G_{xz} by G_{xy} gives

$$\frac{G_{xz}}{G_{xy}} = \frac{G_{uw}}{G_{uv} + G_{mn}} = \frac{H_{vw}}{1 + \frac{G_{mn}}{G_{uv}}} \qquad (13)$$

This estimate of the transfer function is biased only if the extraneous noise in x and y correlates. In an actual application, this bias can be minimized by maximizing the distance between the locations where x and y are measured. Of course, the measurement of x must contain the signal u which is propagating to the far-field. Thus, the location of x must not be upstream of the source.

The method developed for determining unbiased transfer functions involves the use of cross-spectra only (see Eqs. (10) and (13)). The cross-spectra are affected by extraneous noise only if the extraneous noise correlates between the two measurement locations. In contrast, the auto-spectra will always include a contribution from the auto-spectra of the extraneous noise. Thus transfer function estimates that use an auto-spectrum, such as Eq. (5), will always be biased by the extraneous noise.

For application of the preceding to determine transfer functions across components within the core of an engine, a far-field noise measurement is needed in addition to pressure perturbation measurements immediately upstream and downstream of the component of interest. Equation (10) is then used to obtain the transfer function across the internal component. Here, x and y are the respective measurements at the upstream and downstream locations, and z is the far-field measurement. For each component for which the transfer function is desired, a set of internal probes is needed. In order to obtain the transfer function to the far-field, Eq. (13) is used. In this case, z is again the far-field measurement, y is at the core tailpipe exit, and x is sufficiently upstream to minimize the correlation between the extraneous noise at the two internal probes.

Description of Test Data and Data Analysis

The technique just described in the previous section was applied to data obtained from tests on a YF102, a JT15D, and a CF6-50 turbofan engine. These data had been obtained during previous experiments by other investigators. Details of these experiments are given in Refs. 5 to 7. Typically the experiments consisted of obtaining simultaneous recordings from transducers or microphones within the engine core and from far-field microphones. For each engine, the data were obtained over a range of engine operating conditions. Schematics showing the internal measurement locations are presented in Refs. 5 to 7. For the YF102 engine (Ref. 5) two probes were located in the combustor, separated 90° circumferentially, and two were located in the tailpipe, one at the tailpipe inlet and the other at the tailpipe exit. The probe locations for the JT15D engine are shown in Ref. 6. For this engine, one probe was located in the combustor, three at the turbine exit, one at the core nozzle entrance, and two at the nozzle exit. The CF6-50 engine (Ref. 7) had three probes located in combustor, one at the turbine inlet, and one at the tailpipe exit.

A two-channel fast Fourier transform digital signal processor was used to compute the cross-spectra required by Eq. (10) or (13). Typically, these cross-spectra were computed by averaging over 2 minutes of data. Before the transfer functions were computed, the measured cross-spectra were smoothed. The technique used for smoothing is that given in Ref. 8. The technique consists of computing a weighted average of the values of the cross-spectra at five adjacent frequencies. The value of this weighted average is assigned to the center frequency. Further smoothing is accomplished by successive passes through the smoothing routine. The smoothed cross-spectra are then used to compute the transfer function. This transfer function is then also smoothed. This process was used to decrease the fluctuations in the transfer function due to random statistical variations in the measured cross-spectra. This is particularly important for the cross-spectra appearing in the denominator of Eq. (10) or (13). The random variations can, on occasion, cause the value of this cross-spectra to approach zero resulting in large excursions in the computed transfer function. The smoothing process eliminates this problem. The effect of smoothing is shown in Fig. 3. Three computed transfer functions for the tailpipe of the YF102 engine are shown. One is without any smoothing, another with a single pass through the smoothing routine, and the third with five passes through the smoothing routine. As can be seen, the smoothing process removes the fine structure in the transfer function but leaves the coarse structure unaltered. All transfer functions presented in this paper have been smoothed with five passes through the smoothing routine.

Only the transfer function amplitudes are presented. Unless otherwise indicated, these are the amplitudes of measured pressure-to-pressure transfer functions and are presented as amplitude, in dB, against frequency in Hz. The amplitude is computed using the following equation:

$$\text{Amplitude, dB} = 10 \log \left|\text{Transfer Function}\right| \qquad (14)$$

Results

Transfer functions across components within the engine and from the engine to the far-field were computed for three engines: the YF102, the JT15D, and the CF6-50. Typical results are presented. Comparisons showing the effect of specific engine and engine operating conditions are made. Comparisons between transfer functions obtained using the technique developed in this paper, Eq. (10) or (13), and those obtained using the previous technique, Eq. (5), are also made.

Exit to Far-Field Transfer Functions

Transfer functions from the core exit to the far-field were computed for all three engines using Eq. (13). For all three engines, the fluctuating pressure in the combustor was used as the third measured signal, x(t). This location is believed to be sufficiently far upstream to minimize any correlation with the extraneous noise at the core nozzle exit. Since the combustor is a source of core noise, the measurement in the combustor will contain the propagating signal, u(t). Thus, the term G_{mn} in Eq. (13) is assumed to be zero.

In Fig. 4, transfer functions from the core nozzle exit to the 120° far-field microphone are

shown for the three engines, each at two engine speeds. The transfer functions are relatively flat with no general trend with frequency. The transfer functions do, however, exhibit variations with frequency of about 3 dB. It is not presently known if these variations have any physical significance or if they are merely due to low frequency random errors in the transfer function measurement. For all three engines the transfer function at the higher engine speed exceeds that at the lower speed indicating less attenuation of the pressure in going from the engine to the far-field.

Some understanding of the parameters that affect the core exit to far-field transfer function can be obtained from an acoustic power balance between the core exit and the far-field. Equating the acoustic power at the core exit to the far-field acoustic power (after neglecting the low frequency power loss due to conversion of acoustic power into vorticity) gives:

$$\frac{A_E}{\rho_E A_E}\left|P_E\right|^2\left|\frac{Z_E+1}{Z_E}\right|^2\left[(1+M_E)^2-\left|\frac{Z_E-1}{Z_E+1}\right|(1-M_E)^2\right]=\frac{4\pi R^2}{\rho_0 C_0}\left|\overline{P}_F\right|^2 \qquad (15)$$

where $|P_E|$ is the magnitude of the pressure at the core exit and $|\overline{P}_F|$ is the area weighted average far-field pressure magnitude at a distance R from the core exit. Solving (15) for the ratio of the far-field pressure to the core exit pressure gives:

$$\left|\frac{\overline{P}_F}{P_E}\right|=\left\{\frac{A_E}{4\pi R^2}\frac{\rho_0 C_0}{\rho_E C_E}\left|\frac{Z_E+1}{Z_E}\right|^2 \times\left[(1+M_E)^2-\left|\frac{Z_E-1}{Z_E+1}\right|^2(1-M_E)^2\right]\right\}^{1/2} \qquad (16)$$

or

$$10\log\left|\frac{\overline{P}_F}{P_E}\right|=10\log\left(\frac{A_E}{4\pi R^2}\frac{\rho_0 C_0}{\rho_E C_E}\right)^{1/2}+10\log\left\{\left|\frac{Z_E+1}{Z_E}\right|^2\left[(1+M_E)^2-\left|\frac{Z_E-1}{Z_E+1}\right|(1-M_E)^2\right]\right\}^{1/2}$$

The pressure ratio given by Eq. (16) cannot be compared directly with the measured transfer functions since Eq. (16) relates the averaged far-field pressure to the pressure at the core exit while the measured transfer function relates the far-field pressure at a particular radiation angle to the core exit pressure. Equation (16) does indicate the parameters that can affect the core exit to far-field transfer function and does suggest a normalization to account for some of these parameters, i.e., the subtraction of $10\log\left(\frac{A_E}{4\pi R^2}\frac{\rho_0 C_0}{\rho_E C_E}\right)^{1/2}$ from the measured transfer function. This normalization accounts for differences in measurement distance, exhaust area, and ratio of ambient characteristic impedance, $\rho_0 C_0$, to core exit characteristic impedance $\rho_E C_E$. The remaining term in Eq. (16) contains the core exit Mach number, M_E, and the normalized core exit acoustic impedance, Z_E.

Normalized core exit to far-field transfer functions are presented in Fig. 5. In Fig. 5(a), transfer function for the YF102 and JT15D engines are compared at a core exit Mach number of about 0.2. In Fig. 5(b) transfer functions for the YF102, JT15D, and CF6-50 are compared at a core exit Mach number of about 0.55. At both Mach numbers, no consistent variation between engines is observed. The normalization suggested by Eq. (16) appears to have accounted for differences due to engine size.

The effect of far-field angle on the engine-to-far-field transfer function is shown in Fig. 6 using YF102 engine data at 43 percent engine speed. The results are in agreement with what is generally known about core noise. Core noise peaks at 120°, similarly the level of the 120° transfer function exceeds that of the transfer functions at the other angles. The spectral shape of core noise does not vary much with angle and likewise the shapes of the transfer functions do not vary much with the angle.

A striking feature of the transfer functions presented in Fig. 6 is the dip at about 550 Hz. The cause of this dip is not known, but it might be associated with the cut-on of the (1,0) circumferential mode. For the YF102 at 43 percent engine speed, the (1,0) mode cuts on at about 700 Hz at the tailpipe exit and at about 400 Hz in the combustor. The core exit to far-field transfer functions presented in Fig. 6 were computed using Eq. (13). Transfer functions computed using Eq. (13) can be biased if the quantity G_{mn} in Eq. (13) is not zero. For the core exit to far-field transfer function, a nonzero G_{mn} corresponds to correlation between the extraneous noise in the combustor with that at the core exit. If the (1,0) circumferential mode does not radiate to the far-field but still exists within the engine, it would be considered to be extraneous noise within the engine. This could be the case below 700 Hz. At frequencies below 700 Hz, this mode would not be expected to radiate to the far-field, but at frequencies above 400 Hz, this mode should exist in the combustor. Whether the (1,0) circumferential mode exists at the core exit would depend on the cut-on frequencies between the combustor and the core exit. Even if this mode is cut-off over a portion of the distance between the combustor and the core exit, it might still exist at the core exit with enough strength to bias the computed transfer function. The lack of a similar dip in the JT15D transfer functions, Fig. 4, can be explained by the fact that the (1,0) mode is not cut-on at the core exit of this engine at frequencies below 1100 Hz. Some evidence of a dip exists in the CF6-50 core exit to far-field transfer function at 63 percent speed at about 200 Hz, which corresponds to the cut-on frequency for the (1,0) mode at the core exit of this engine. However, no corresponding dip occurs in the transfer function at 93 percent engine speed.

Tailpipe Transfer Functions

Transfer functions a ross the tailpipes of the YF102 ahd JT15D engines were determined for several engine speeds. Transfer functions across the tailpipe of the CF6 engine could not be computed because only one probe was located in the CF6 tailpipe. The tailpipe transfer functions were computed using Eq. (10). For most of the data, the measurement with the 120° far-field microphone is used as the third signal, z(t). The effect of using measurements at other far-field locations is also shown.

In Fig. 7, transfer functions across the nozzle portion of the JT15D tailpipe are shown for several engine speeds. The probe locations and nozzle geometry for these transfer functions are shown in Fig. 8. Since little difference exists between the curves in Fig. 7, it appears that the flow and temperature variations associated with changes in engine speed are insufficient to produce significant changes in the tailpipe transfer function.

Transfer functions across the tailpipe of the YF102 engine are shown in Fig. 9 for several engine speeds. Here, some variation with speed exists but no consistent trend can be observed.

The transfer functions presented in Figs. 7 and 9 were computed using the measurement with the 120° far-field microphone as the third measurement signal, z(t). In Fig. 10, tailpipe transfer functions using measurements at different far-field locations are compared. Except for random variations, the tailpipe transfer function should be independent of which far-field location is used. Looking at Fig. 10(a), for the YF102 at 43 percent engine speed, this appears to be the case. The curves are quite similar with no consistent trend with far-field angle being evident. At the 95 percent engine speed, Fig. 10(b), while the random variation has increased somewhat, the curves are still similar with differences in level of about 3 dB.

Turbine Transfer Functions

Transfer functions across the turbines of the three engines are presented in Fig. 11. For all three engines a measurement from a combustor probe is used as the upstream signal. For the YF102 and JT15D engines measurements from probes a short distance downstream of the turbine are used as the downstream signal. For the CF6-50 engine, the only measurement downstream of the turbine was at the tailpipe exit and that was used as the downstream signal. Thus the CF6-50 turbine transfer function includes the transfer function across the CF6 tailpipe. For all three engines, the measurement with the 120° far-field microphone was used as the third signal.

As can be seen in Fig. 11, no significant trend with engine speed is obvious, but differences from engine to engine do exist, both in the shape and level of the transfer functions. The levels of the YF102 and JT15D turbine transfer functions are about the same while that of the CF6-50 is about 10 dB lower. It is interesting to note that the core noise prediction technique of Ref. 9 includes a term for the attenuation across the turbine. The term used contains the fourth power of the temperature difference across the turbine. (Note: the fourth power is for the attenuation of intensity; for pressure, this corresponds to a second power.) Comparing the values of this term, for the three engines, indicates that the turbine transfer functions for the YF102 should be 1.5 dB below that of the JT15D and that for the CF6-50 should be 6 dB below the JT15D. Any remaining difference in overall turbine transfer function level between the CF6 engine and the YF102 and JT15D engines may be due to the inclusion of the CF6 tailpipe.

Comparison of New and Old Techniques

Comparisons of transfer functions obtained using the technique developed in this report, Eq. (10) or (13), with those obtained using the old technique, Eq. (5), are presented in Figs. 12 to 14. In Figs. 12(a) to (c), exit to far-field transfer functions are compared. For the JT15D at 40 percent engine speed, Fig. 12(a), the transfer functions obtained from using the two techniques agree at low frequency but differ by about 5 dB at higher frequencies. For the CF6 engine, the differences are more substantial, being from 2.5 to 12.5 dB at 63 percent engine speed and from 7.5 to 15 dB at 94 percent engine speed. In all cases, the transfer functions computed using Eq. (5) indicate more attenuation. This difference is due to the presence of extraneous noise in the measurement at the tailpipe exit giving rise to a nonzero value of G_{mm} in the denominator of Eq. (5). In Fig. 13, a comparison of the two estimates of the YF102 tailpipe transfer functions is made. Again more attenuation is indicated by the transfer function obtained using Eq. (5). An example showing large differences, not only in level but also in shape, between the two transfer function estimates is shown in Fig. 14 for the YF102 turbine. The dips in the transfer function computed using Eq. (5) are probably associated with extraneous noise due to the cut-on of higher order modes in the combustor.

Summary and Conclusions

A technique was developed in this paper to provide a method for computing transfer functions in the presence of extraneous noise. The application of this technique to turbofan engine core noise transmission resulted in a set of measured transfer functions across engine components and to the far-field. The fact that the resulting transfer functions are well behaved and consistent with existing knowledge of core noise propagation provides confidence in the method developed. The transfer functions presented in this paper, especially if supplemented with measured transfer functions from other engines, should add much to the understanding of core noise transmission. By analyzing the transmission across individual components, the effect of these components on the total transmission can be assessed.

Transfer functions from the core exit to the far-field showed that the attenuation from the core exit to the far-field decreased with Mach number. Subtracting $10 \log \left(\frac{A_E}{4\pi R^2} \frac{\rho_o c_o}{\rho_E c_E} \right)^{1/2}$ from the measured core exit to far-field transfer functions appears to adequately normalize the transfer function for engine core exhaust area, measurement distance, and characteristic impedance effects.

Tailpipe transfer functions varied little with engine speed. Also they were not sensitive to the location of the far-field microphone used to compute these transfer functions.

Turbine transfer functions varied significantly from engine to engine both in shape and level. The level of the CF6-50 turbine transfer functions was about 10 dB below that of the JT15D and YF102 engines. A difference of 6 dB is calculated from the turbine attenuation term in some existing core noise prediction formulae.

References

1. von Glahn, U. H., and Groesbeck, D. E., "Comparison of Predicted Engine Core Noise with Current and Proposed Aircraft Noise Certification Requirements," NASA TM-82659, 1981.

2. Strahle, W. C., Muthukrishnan, M., Neale, D. H., and Aggarwal, S. K., "Combustion Noise Prediction: Energy/Vorticity Effects," Georgia Institute of Technology, FAA-RD-79-1, Mar. 1979.

3. Krejsa, E. A., "New Technique for the Direct Measurement of Core Noise from Aircraft Engines," NASA TM-82634, 1981.

4. Bendat, J. S., and Piersol, A. G., Engineering Applications of Correlation and Spectral Analysis, John Wiley and Sons, New York, 1980, pp. 85-92.

5. Reshotko, M., Karchmer, A., Penko, P., and McArdle, J., "Core Noise Measurements on a YF-102 Turbofan Engine," NASA TM X-73587, 1977.

6. Reshotko, M., and Karchmer, A., "Core Noise Measurements from a Small, General Aviation Turbofan Engine," NASA TM-81610, 1980.

7. Doyle, V. L., and Moore, M. T., "Core Noise Investigation of the CF6-50 Turbofan Engine," General Electric Company, Cincinnati, OH, R79AEG395, Jan. 1980. (NASA CR-159749.)

8. Salikuddin, M., Brown, W. H., Ramakrishnan, R., and Tanna, H. K., "Refinement and Application of Acoustic Impulse Technique to Study Nozzle Transmission Characteristics," Lockheed-Georgia Company, Marietta, Georgia, LG82ER0115, Feb. 1983. (NASA CR-3656.)

9. Matta, R. K., Sandusky, G. T., and Doyle, V. L., "G. E. Core Engine Noise Investigation - Low Emission Engines," General Electric Company, FAA-RD-77-4, Feb. 1977.

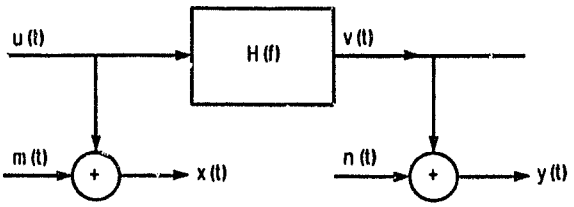

Figure 1. - Single input single output system with extraneous noise (Fig. 4.2 of reference 4).

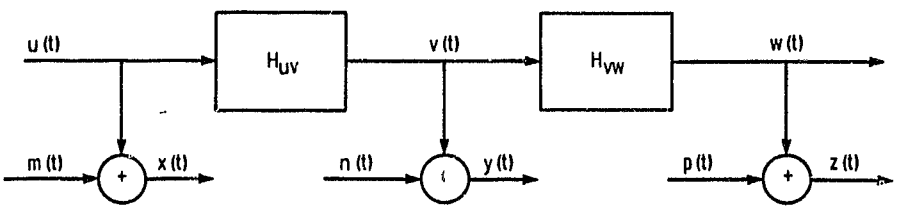

Figure 2. - Block diagram of system used to remove bias from transfer function measurements.

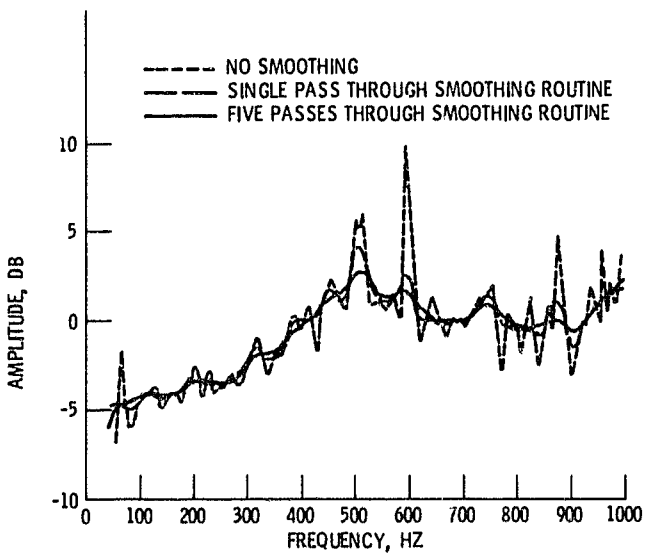

Figure 3. - Effect of smoothing on the YF102 tailpipe transfer function, 43% engine speed.

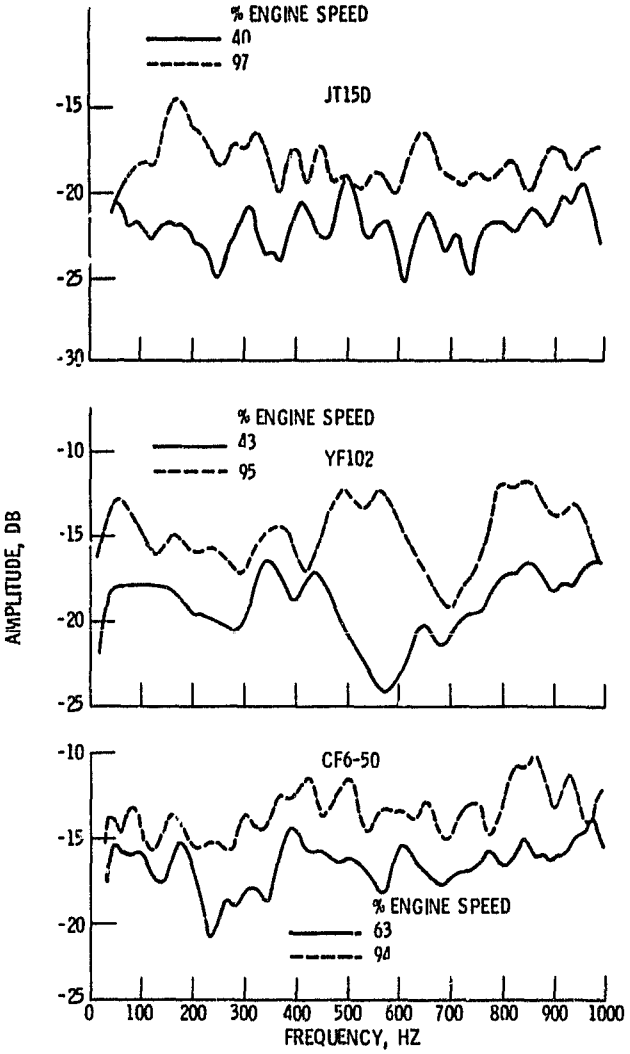

Figure 4. - Nozzle exit to far-field transfer functions. Microphone angle, 120^0 from engine inlet centerline.

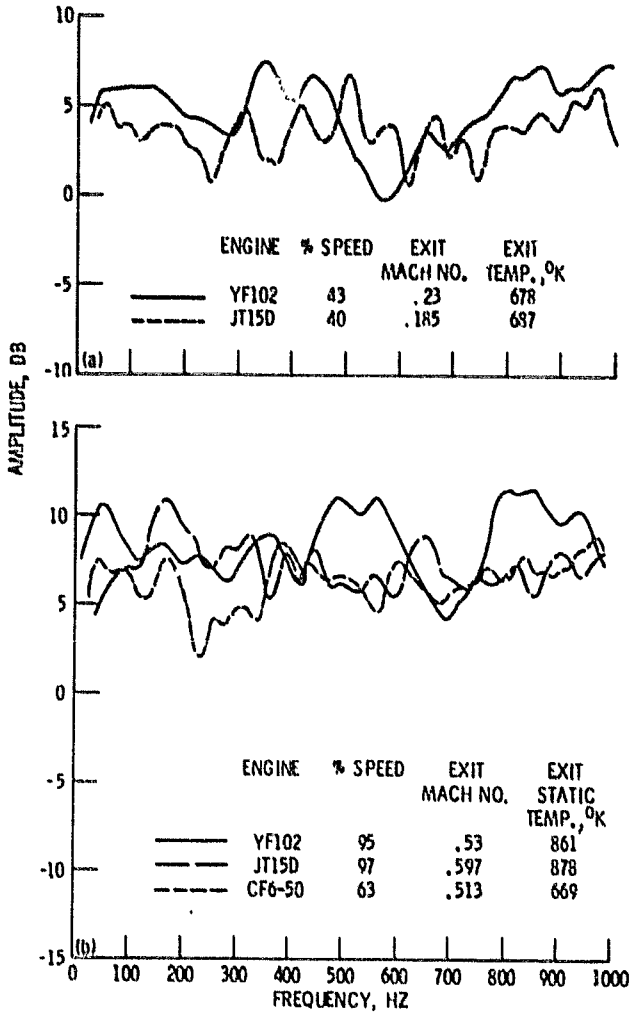

(a) Mach no. = .2.
(b) Mach no. = .5 to .6.

Figure 5. - Engine to 120° far-field transfer functions adjusted by subtracting 10 log $\left(\frac{A_E}{4\pi R^2} \cdot \frac{\rho_0 Co}{\rho_E CE}\right)^2$ from the measured transfer functions.

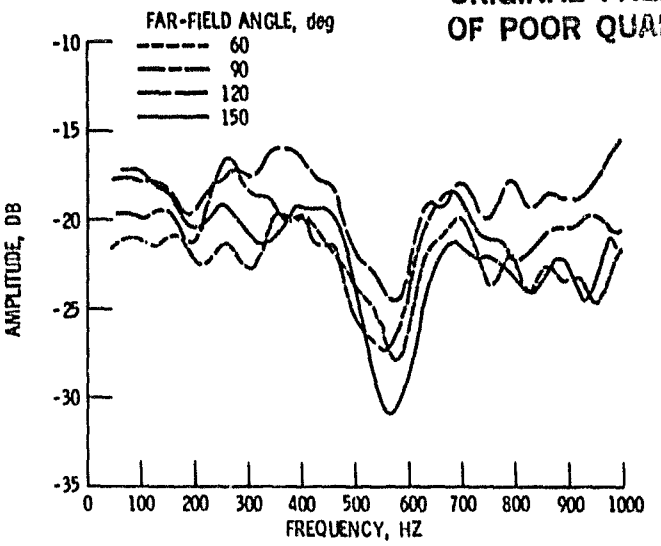

Figure 6. - Effect of far-field angle on engine to far-field transfer functions. YF102 engine. 43% engine speed.

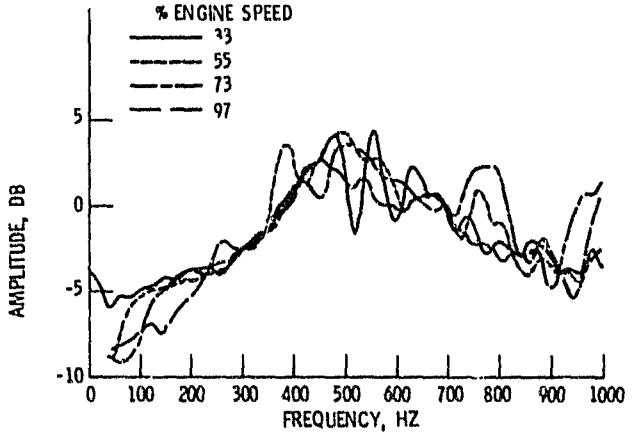

Figure 7. - Effect of engine operating condition on JT15D nozzle transfer functions.

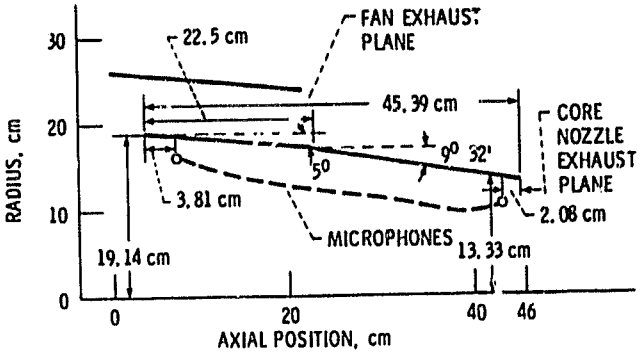

Figure 8. - JT15D nozzle geometry and probe locations.

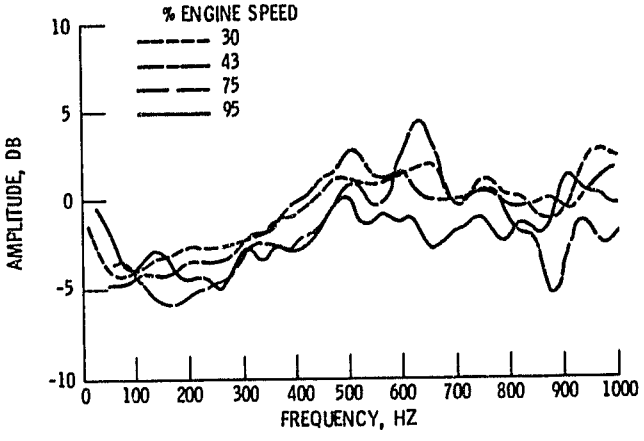

Figure 9. - Effect of engine operating condition on the YF102 tailpipe transfer function.

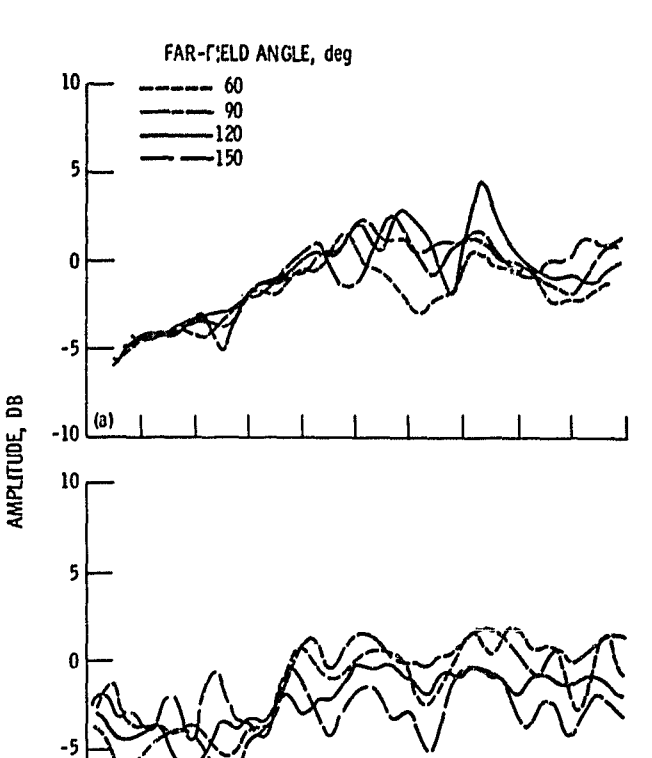

(a) 43% engine speed.
(b) 95% engine speed.

Figure 10. - Effect of far-field measurement location on tailpipe transfer function, YF102 engine.

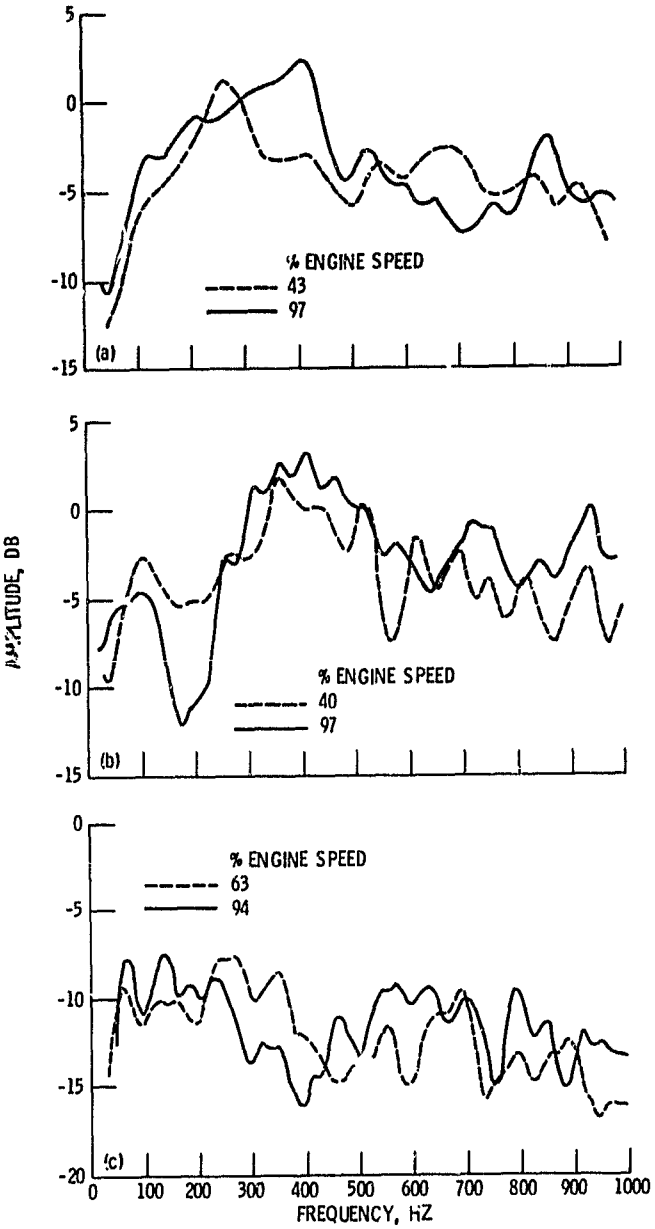

(a) YF102 engine.
(b) JT15D engine.
(c) CF6-50 engine.

Figure 11. - Turbine transfer functions.

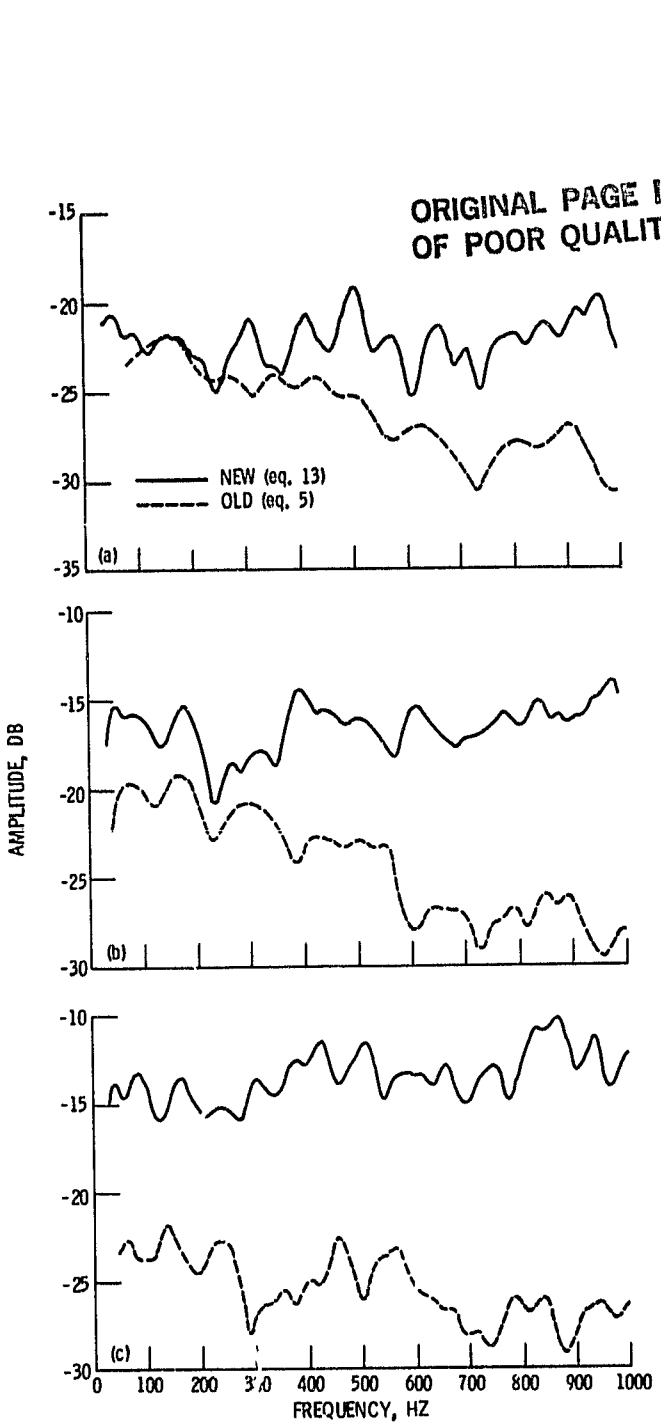

(a) JT15D engine, 40% engine speed.
(b) CF6-50 engine, 63% engine speed.
(c) CF6-50 engine, [illegible]% engine speed.

Figure 12. - Comparison of transfer function computation techniques on exit to far-field transfer functions.

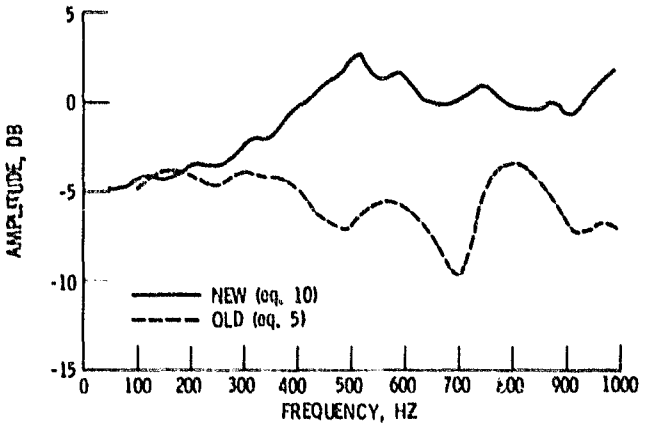

Figure 13. - Effect of computation method on the tailpipe transfer function of the YF102, 43% engine speed.

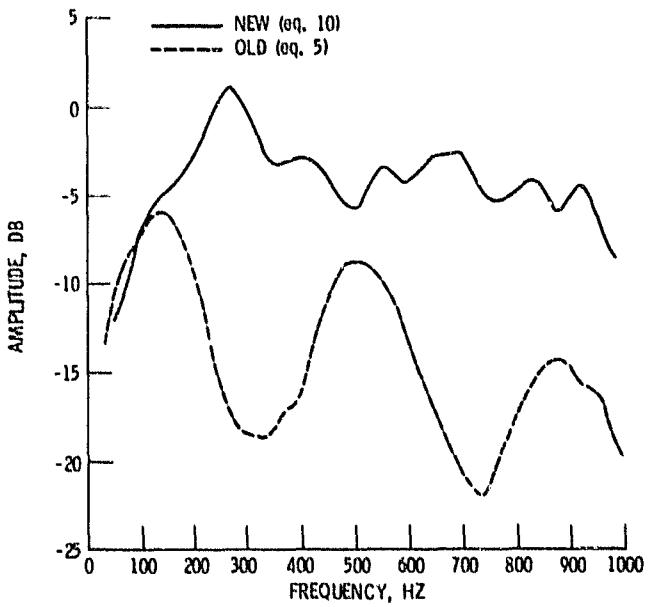

Figure 14. - Effect of computation technique on the YF102 turbine transfer function, 43% engine speed.